

Non-Thermal Chemistry in Diffuse Clouds with Low Molecular Abundances¹

J. Zsargó^{2, 3} and S.R. Federman²

ABSTRACT

High quality archival spectra of interstellar absorption from C I toward 9 stars, taken with the Goddard High Resolution Spectrograph on the *Hubble Space Telescope*, were analyzed. Our sample was supplemented by two sight lines, 23 Ori and β^1 Sco, for which the C I measurements of Federman, Welty, & Cardelli were used. Directions with known CH⁺ absorption, but only upper limits on absorption from C₂ and CN, were considered for our study. This restriction allows us to focus on regions where CH⁺ chemistry dominates the production of carbon-bearing molecules.

Profile synthesis of several multiplets yielded column densities and Doppler parameters for the C I fine structure levels. Equilibrium excitation analyses, using the measured column densities as well as the temperature from H₂ excitation, led to values for gas density. These densities, in conjunction with measurements of CH, CH⁺, C₂, and CN column densities, provided estimates for the amount of CH associated with CH⁺ production, which in turn set up constraints on the present theories for CH⁺ formation in this environment. We found for our sample of interstellar clouds that on average, 30–40% of the CH originates from CH⁺ chemistry, and in some cases it can be as high as 90%.

A simple chemical model for gas containing non-equilibrium production of CH⁺ was developed for the purpose of predicting column densities for CH, CO, HCO⁺, CH₂⁺, and CH₃⁺ generated from large abundances of CH⁺. Again, our results suggest that non-thermal chemistry is necessary to account for the observed abundance of CH and probably that of CO in these clouds.

Subject headings: ISM:abundances - ISM:molecules - ultraviolet: ISM

¹ Based on observations obtained with the NASA/ESA *Hubble Space Telescope* through the Space Telescope Science Institute, which is operated by the Association of Universities for Research in Astronomy, Inc., under NASA contract NAS5-26555.

² Department of Physics and Astronomy, University of Toledo, Toledo, OH 43606.

³ Department of Physics and Astronomy, The Johns Hopkins University, Baltimore, MD 21218.

1. Introduction

Carbon is rarely found in the form of C I in the general interstellar medium (ISM). In the hot, ionized part of the ISM (like the interior of superbubbles), it is highly ionized, while in the warm neutral regions it is mainly in the form of C II. As the cloud gets colder the recombination of C II and the transition from C I to CO appears almost simultaneously (Hollenbach & Tielens 1999), leaving little room for C I as the dominant form of carbon. The diffuse clouds where this double transition usually occurs are very important for understanding the nature of atomic and molecular chemistry in the ISM. It is here where the important nonthermal effects, dissipation of turbulence (Duley et al. 1992; Falgarone, Pineau des Forêts, & Roueff 1995; Hogerheijde et al. 1995; Joulain et al. 1998; Pety & Falgarone 2000) and MHD waves (e.g., Draine & Katz 1986; Pineau des Forêts et al. 1986; Gredel, van Dishoeck, & Black 1993; Charnley & Butner 1995; Federman et al. 1996a), can seriously alter the chemical composition of the clouds. For example, it is not possible to understand the observed abundance of CH^+ without taking into account these effects.

Our first objective is to derive the gas density and the kinetic temperature for such diffuse clouds. We infer this information from the observed populations among fine structure levels of the electronic ground state of C I. We searched the *Hubble Space Telescope* (*HST*) archive for spectra of bright stars known to show weak or moderate molecular absorption to minimize the effects of denser molecular cores. In all, we found nine suitable target stars; their properties from the Simbad database are listed in Table 1. The reddenings are from Savage et al. (1977). We included 23 Ori and β^1 Sco (not listed in Table 1) in our sample with C I column densities from Federman et al. (1997).

The target stars are located in Taurus, Perseus, Orion, Scorpius, and Ophiuchus, with the exception of HD 112244. The general environment toward these stars is well characterized through numerous studies. η Tau, for example, is one of the brightest members of the Pleiades (White 1984). Krelowski, Megier, & Strobel (1996) found two absorbing components toward the Perseus OB2 association, but simple molecules (CH, CN) could be detected only in one of them. UV observations of Martin & York (1982) and Vidal-Madjar et al. (1982) detected several absorption components toward the Perseus association. With the exception of one cold component, these were too weak and too hot to be observable in neutral carbon. The temperatures deduced by Trapero et al. (1992) from interstellar K I absorption toward stars in Perseus are in general agreement with the results of this study.

de Geus (1992) described the immediate vicinity of the Scorpio-Centaurus region in detail. He found that the ISM has been shocked and disturbed by the strong winds of O and B stars and past Type II supernovae from the numerous OB associations located here. A CO survey of the Ophiuchus region by de Geus, Bronfman, & Thaddeus (1990) found

5 main and several weaker cloud components. It is likely, however, that some of them are dense molecular cores not relevant for this study. High resolution spectroscopy of Na I D and K I $\lambda 7699$ lines by Kemp, Bates, & Lyons (1993) revealed only 3 components, two stronger and one weak, in general agreement with our findings of two components. The more recent atomic surveys of Welty, Hobbs, & Kulkarni (1994) and Welty & Hobbs (2000) also indicate that our C I measurements probe the strongest components toward our sample of stars. *Copernicus* observations of σ Scorpii (Allen, Snow, & Jenkins 1990) revealed 4 components based primarily on H₂ lines.

The main objective of this study is to obtain information on the importance of non-equilibrium CH⁺ chemistry for production of CH and CO in diffuse clouds. These molecules can be produced in very different environments. In the denser portions of a cloud they are involved in a complex thermal chemistry, while in warmer and more tenuous portions they are produced via CH⁺. Since any line of sight can involve several clouds and cloud sections, the inferred quantities and parameters are likely the result of several environments. If one can set up reasonable estimates of the contributions from the different environments, further constraints on the physical processes underlying nonthermal CH⁺ chemistry can be established.

We follow two approaches in our study. On the one hand, we estimate the amount of CH produced in denser regions (with equilibrium chemistry) and establish lower and upper limits on CH produced by the molecular chemistry. The difference between our limits and the observations should come from non-equilibrium chemistry, and this has to be accommodated by any model attempting to explain CH⁺ chemistry. On the other hand, we calculate CH and CO abundances arising from CH⁺ in diffuse clouds using the model of Federman et al. (1996a) to have a rough estimate of the amount coming from non-equilibrium chemistry. As an improvement on the models in Federman et al. (1996a), we use increased effective temperatures not only for ions, but also for neutrals directly produced by ion-ion or ion-neutral reactions. The effects on CH were noted by Gredel et al. (1993) and described in detail by Bucher & Glinski (1999).

Details of the data reduction and measurements are discussed in Section 2. The gas densities and temperatures were inferred from relative populations obtained by fitting synthetic spectra to the observations. We discuss this analysis in Section 3 and describe how the gas densities and temperatures were inferred from C I excitation in Section 4. We present the calculation of molecular abundances in Sections 5 and 6 for the equilibrium and non-equilibrium chemistry, respectively. We discuss our result briefly in Section 7 and summarize them in Section 8.

2. Measurements and Data Reduction

We retrieved observations for 9 new lines of sight from the *HST* archive; most were acquired at medium resolution (MR; $R = \frac{\lambda}{\Delta\lambda} = 20,000$) and a handful were taken at high resolution (HR; $R = 100,000$). These spectra covered several C I multiplets and forbidden lines between 1150 Å and 1700 Å. The datasets that were retrieved from the *HST* archive and used in our study are presented in Table 2.

We used the standard IRAF STSDAS package to cross-correlate and coadd the subexposures of the archival spectra. The most serious concern was an error in the background correction on some of our preprocessed data. We detected this error on all of our HR spectra containing the $\lambda 1260$ multiplet of C I. The flux level of a strongly saturated line, such as those of S II and Si II, should be zero at line center; however, in some cases we measured negative or small positive values, clearly indicating an erroneous background correction. We could then apply an additional correction to compensate for the effect. We never encountered this problem on MR spectra although we had saturated lines in some cases, probably because scattered light was more easy to quantify in grating spectra.

After calibration and data reduction, the components in the neutral carbon lines were identified and the continuum of the background star was removed (continuum placement) by fitting it to a low order polynomial. The continuum placement turned out to be difficult for some multiplets, due to blending of several lines or simply because the lines were saturated. For example, in the vicinity of multiplet $\lambda 1260$, Si II and Fe II lines seriously affected the continuum placement.

Following line identification and continuum placement, the Doppler shift (relative to the laboratory wavelength) and equivalent width (W_λ) of neutral carbon lines were measured. In some cases, only upper limits could be extracted from the average Full Width at Half Maximum (FWHM) of the instrumental function and the root mean square (rms) average of the noise in the stellar continuum ($W_\lambda \leq 2 \times \text{FWHM} \times \text{rms}$). The measured values of W_λ are listed in Tables 11-19 in the Appendix for comparison with results of other investigations.

The *HST* data for ϵ Per and ω^1 Sco were supplemented with spectra for additional lines acquired with the *Copernicus* satellite. These coadded spectra were obtained from the Multiwavelength Archive at the Space Telescope Science Institute (MAST). All spectra for each of the two directions were analyzed together.

3. C I Column Densities and Doppler Parameters

The column densities (N) and the Doppler parameters (b -values) that describe the absorbing components along each line of sight were determined by fitting synthetic profiles to the observed spectra. The synthetic fluxes were compared to the observations and the set of initial parameters was adjusted by a χ^2 minimization until a satisfactory fit to all observed spectra for a sight line could be achieved. Our approach was a modified second order gradient method, taken from Bevington & Robinson (1992). The program was tested by reproducing the results of curves of growth. We estimated the errors for the inferred parameters to be $\approx 10\%$, based on the goodness of the continuum placement and the noise in the spectra. The effects of other potential sources of error were negligible. For oscillator strengths, we used those from the compilation of Morton (1991), updated with our more recent astronomical determinations (Zsargó, Federman, & Cardelli 1997; Federman & Zsargó 2001).

Throughout the synthesis we used a Gaussian instrumental function with a FWHM of $\approx 3 \text{ km s}^{-1}$ and $\approx 15 \text{ km s}^{-1}$ for HR and MR spectra, respectively. The exact values of FWHM were calculated for each spectrum from the wavelength dependence in the resolution of Echelle-A and G160M (described in the instrumental handbook for the GHRS).

The results of the profile syntheses are shown in Table 3. To demonstrate the quality of fits that could be achieved by this procedure, we display observed and synthesized spectra for 1 Sco in Figure 1. The differences between the observed and model spectra in the Figure are well within the continuum noise for all C I multiplets. The HR spectra of λ Ori, 1 Sco, δ Sco, and σ Sco revealed that there are at least two components in C I absorption along these sight lines. The two components toward 1 Sco, for example, are clearly visible in the HR spectra of C I $\lambda 1328.83$ in Figure 1. We could not discern multiple components toward most sight lines for which only MR spectra were available. The only exception is HD 112244 where the large separation ($\approx 24 \text{ km s}^{-1}$) between the components was easily recognizable. The main absorption component (Component A) for the lines of sight in Table 3 are very well defined. The uncertainties in their columns and b -values are dominated by the errors in the continuum placement and by the signal-to-noise ratio of the spectra. The parameter values for the secondary components (Component B), on the other hand, are not defined very well. Often, we had to keep some parameters fixed during the synthesis in order to achieve reasonable values for the column densities, or else, only upper limits of N could be provided.

Comparison between our line parameters and those extracted from high and ultra-high resolution measurements of atoms and molecules shows good correspondence. There are four sight lines with one C I component, η Tau, ϵ Per, π Sco, and ω^1 Sco. The sight lines toward η Tau and ϵ Per indicate but one component in K I (Welty & Hobbs 2000) with b -values

of about 1 km s^{-1} . Presumably, the larger b -values in C I arise because this atom probes more widely distributed material. For π Sco and ω^1 Sco, Welty et al. (1994) and Welty & Hobbs (2000) see multiple components in Na I D and K I, respectively. Here, our lower resolution measurements could not distinguish absorption from the stronger, closely spaced components. The b -values for the $J = 0$ lines reflect this. The narrower b -values for lines from $J = 1$ and 2 are likely the result of their sampling only the strongest component, a smaller portion of the line of sight, or both.

A similar pattern emerges for the sight lines with two C I components. The $\approx 12 \text{ km s}^{-1}$ separation seen toward λ Ori comes from the complexes discerned in Na I D measurements (Hobbs 1974; Welty & Hobbs 2000). Toward HD 112244, the two components about 24 km s^{-1} apart are also present in CH spectra (Danks, Federman, & Lambert 1984). For 1 Sco, the correspondence is seen in Na I D complexes (Welty et al. 1994; Welty & Hobbs 2000), separated by about 7 km s^{-1} . The same applies to the two C I components ($\Delta v \approx 5 \text{ km s}^{-1}$) toward δ Sco, which are present in Na I D and K I (Welty & Hobbs 2000) and CH⁺ (Crane, Lambert, & Sheffer 1995). Finally, the 9 km s^{-1} separation in components toward σ Sco is seen in Na I D and K I (e.g., Welty & Hobbs 2000).

4. Excitation Analysis

We used the column densities found from the profile syntheses to infer gas densities and temperatures for the gas containing C I. To do so we assumed steady-state detailed balance among the fine structure levels $J = 0, 1$, and 2 of neutral carbon. Two independent number density ratios can be established. These are

$$\frac{n_{J=2}}{n_{J=0}} = \frac{R_{0,2}(A_{1,0} + R_{1,0} + R_{1,2}) + R_{1,2}R_{0,1}}{(A_{2,1} + R_{2,1} + R_{2,0})(A_{1,0} + R_{1,0} + R_{1,2}) - R_{1,2}(A_{2,1} + R_{2,1})} \quad (1)$$

and

$$\frac{n_{J=1}}{n_{J=0}} = \frac{R_{0,1}(A_{2,1} + R_{2,1} + R_{2,0}) + R_{0,2}(A_{2,1} + R_{2,1})}{(A_{2,1} + R_{2,1} + R_{2,0})(A_{1,0} + R_{1,0} + R_{1,2}) - R_{1,2}(A_{2,1} + R_{2,1})} \quad (2)$$

where the terms $R_{i,j}$ are defined by

$$R_{i,j} = \sum_k \gamma_{i,j}^k n_k + G_{i,j} \quad (3)$$

The quantities $\gamma_{i,j}^k$ are the collisional excitation or de-excitation rate coefficients through collision with species k and $G_{i,j}$ are the ultraviolet radiative pumping rates between fine structure levels i and j . In eqns. 1 and 2, the quantity $A_{i,l}$ is the far infrared spontaneous decay rate from level i to level l . Variables n_k are the number density of species k . For our

lines of sight, collisions with H, He, and H₂ were considered, since they are the most abundant species in diffuse interstellar clouds. The C I collisional de-excitation rate coefficients are listed in Table 4. The corresponding excitation rates can be calculated by the formula

$$\gamma_{j,i}^k = \gamma_{i,j}^k \frac{2i+1}{2j+1} e^{-T_{i,j}/T} , \quad (4)$$

where $kT_{i,j}$ and T are the energy between states i and j and the gas temperature, respectively. The rates for C I collisions with H₂ and H were taken from Schröder et al. (1991) and from Launay & Roueff (1977), respectively. The collisional rates for He were from Lavendy, Robbe, & Roueff (1991) and Staemmler & Flower (1991). Radiative pumping was neglected in our analysis because it has a negligible effect on the populations, unless the ultraviolet field is at least 10 times the strength of the average interstellar field.

If the clouds have close to uniform density and chemical composition, then

$$n_k \approx \frac{N_k n}{N_H + N_{H_2} + N_{He}} , \quad (5)$$

$$\frac{n_{J=1}}{n_{J=0}} \approx \frac{N_{J=1}}{N_{J=0}} \quad \text{and} \quad \frac{n_{J=2}}{n_{J=0}} \approx \frac{N_{J=2}}{N_{J=0}} ,$$

where the N -s are the column density of species k , hydrogen, H₂, helium, or a C I fine structure level, and n is the gas density. We calculated the fractional abundances for H and H₂ using column densities from Savage et al. (1977) and we assumed that 10% of the material is He for all lines of sight.

After substituting eqn. 5 in eqns. 1 and 2, one has two equations for the unknown temperature and gas density. Unfortunately, the temperature and density solutions for eqns. 1 and 2 are not unique. One can find many density-temperature pairs to satisfy these equations for a specific $\frac{n_{J=1}}{n_{J=0}}$ or $\frac{n_{J=2}}{n_{J=0}}$ ratio. As a further complication, the uncertainties in the C I column densities introduce uncertainties in the C I level ratios; therefore, a density range rather than a given value satisfies eqn. 1 or 2 for a temperature. As a consequence of this ambiguity, numerous density-temperature pairs simultaneously satisfy eqns. 1 and 2. One needs independent density or temperature estimates to further confine the solutions.

The density–temperature solutions of eqns. 1 and 2 are displayed in Figure 2 for the main components of each sight line. The C I excitation analysis was supplemented by the temperature estimates of Savage et al. (1977) which were determined by H₂ excitation analysis for the sight lines. Since the H₂ temperatures of Savage et al. (1977) are valid only for the main components, we did not perform the C I excitation analysis for the secondary components.

The sole exception is HD 112244 where the two components are fairly similar; therefore, the temperature estimate of Savage et al. (1977) most likely applies to both components. In Figure 2, each C I ratio resulted in two density–temperature curves corresponding to the maximum and minimum ratios that were allowed by the uncertainties in the C I column densities. Any density-temperature point between the solid or the dashed curves in Figure 2 is consistent with the observed C I $J=0$ and 1 or the $J=0$ and 2 column densities. Then, the region that is between all four curves contains all density-temperature pairs that are the simultaneous solutions to eqns. 1 and 2. However, Figure 2 also shows that the temperature values are not well defined for most sight lines. The allowed temperatures range between 30 and 200 K, and can be confined only by the estimates of Savage et al. (1977). For simplicity, we accepted as solutions all the density-temperature pairs in Figure 2 that lie within the thick rectangles. These regions provide the smallest independent density and temperature ranges that satisfy both eqns. 1 and 2 for the observed C I ratios and consistent with the H_2 excitation temperatures. The derived density and temperature ranges are listed in Table 5. In the case of η Tau, we chose to list only an upper limit for the density, since the lower limit is essentially zero.

5. CH Production in Moderately Dense Regions

To estimate the amount of CH produced in the denser regions in our sight lines, we followed the method described in detail by Federman et al. (1997). In their work, they only used the most important processes to find the analytic expression

$$x(\text{CH}) = \frac{0.67 k_1 x(\text{C}^+) x(\text{H}_2) n}{G(\text{CH})} \quad (6)$$

that describes the CH fractional abundance. In eqn. 6 and all the following equations, k_i denotes the rate coefficient for reaction i and the fractional abundance of a species y is $x(y) = n(y)/(n(\text{H}) + 2n(\text{H}_2))$. The terms n , $n(y)$, and $G(y)$ are the gas density, number density of species y , and the photodissociation rate for species y , respectively. The photodissociation rate includes grain attenuation of ultraviolet radiation which is approximated by $\tau_{UV} = 2A_V$ (Federman et al. 1994). For the sight lines in Scorpius, which have larger ratios of total to selective extinction, a value of $1.4A_V$ was adopted. One can invert eqn. 6 and solve for n using the observed CH abundance for a comparison between the densities derived from C I excitation. We can also constrain our results for CH, using available upper limits for $N(\text{C}_2)$ and $N(\text{CN})$. In equilibrium, the fractional abundances are given by the following expressions (Federman et al. 1997):

$$x(\text{C}_2) = \left(\frac{1}{0.67} \right) \left(\frac{k_2}{k_1} \right) \left(\frac{G(\text{CH})}{G(\text{C}_2)} \right) \left(\frac{x(\text{CH})}{x(\text{H}_2)} \right) x(\text{CH}) \quad (7)$$

and

$$x(\text{CN}) = \left(\frac{1}{0.67} \right) \left(\frac{k_4 x(\text{N}) + 0.045 k_5 x(\text{C}^+)}{k_1 x(\text{C}^+)} \right) \left(\frac{G(\text{CH})}{G(\text{CN})} \right) \left(\frac{x(\text{CH})}{x(\text{H}_2)} \right) x(\text{CH}). \quad (8)$$

The rate coefficients and photodissociation rates used in this analysis are given in Table 6. A detailed description of these coefficients is given by Federman et al. (1994) with updates in Pan, Federman, & Welty (2001). Table 7 lists the necessary fractional abundances and τ_{UV} calculated from $E(B - V)$ values of Savage et al. (1977). The data for H_2 and the carbon-bearing molecules, CH , C_2 , and CN , are from Savage et al. (1977) and Federman et al. (1994), respectively. The CO abundances are from recent analyses of *Copernicus* spectra (Crenny & Federman 2001, private communication). We used the CH^+ abundances of Federman (1982), Lambert & Danks (1986), and Price et al. (2001). The data for $x(\text{C}^+)$ are from Sofia et al. (1997), $x(\text{O})$ from Meyer, Jura, & Cardelli (1998), and $x(\text{N})$ from Lugger et al. (1978) and York et al. (1983).

We estimated the gas densities necessary to reproduce the observed CH columns in an environment in thermal equilibrium by inverting eqn. 6 and using the data in Tables 6 and 7. Such environments are very different from those required to produce the observed amount of CH^+ . The calculated upper limits on densities, as expected, are much larger than those found from C I excitation (see Section 5). The sole exception is σ Sco, where the two densities are marginally consistent with each other. Since we chose lines of sight with no detectable C_2 and CN absorption, densities of several thousand cm^{-3} are not realistic, and the values inferred from C I excitation are more appropriate. The clear inconsistency resulting from the two density calculations is a strong indication that non-equilibrium CH chemistry is important toward these stars. This contrasts with the results for the molecule-rich gas toward ζ Oph (Lambert et al. 1994) where the above calculation and the observations gave similar results.

Using $x(\text{C}_2)$ or $x(\text{CN})$ as well as N_{total} from Table 7, we can estimate the column densities of CH associated with the equilibrium chemistry from eqns. 7 or 8. Then, a lower limit on the amount of CH associated with the non-equilibrium CH^+ chemistry can be imposed by comparing the calculated amounts to the observed column densities. On the other hand, if we use the densities derived from C I excitation in eqn. 6, an upper limit on the amount of CH produced via CH^+ can be obtained. In Figure 3 we display the results, normalized to the observed column of CH^+ . The triangles and downward-pointing arrows represent the measured values and upper limits of the $N(\text{CH})/N(\text{CH}^+)$ ratios, respectively. Ranges indicate the normalized CH columns that are likely to be associated with the non-equilibrium CH^+ chemistry. Again, the results in Figure 3 strongly suggest that non-equilibrium chemistry is indeed very important for the production of CH in molecule-poor sight lines, and in some cases, like that of 23 Ori, it is the dominant source for this molecular species.

A larger contribution from the non-equilibrium CH^+ chemistry would be necessary if CH is effectively destroyed by reactions with atomic hydrogen (reaction 30 in Table 8) in the moderately dense regions along our sight lines. This reaction is thought to be suppressed by a reaction barrier (e.g., Mitchell & Deveau 1983); however, recent quantal calculations (Harding, Guadagnini, & Schatz 1993; van Harrevelt, van Hemert, & Schatz 2002) suggest that this may not be the case. Unfortunately, the rate coefficient for the reaction is not well defined for the gas temperatures relevant to the diffuse ISM, and the value of $x(\text{H})$ in the moderately dense regions is not known – only line of sight averages are available. Therefore, the importance of the reaction, $\text{CH} + \text{H} \rightarrow \text{C} + \text{H}_2$, could not be judged properly and the reaction was not included in eqns. 6 – 8. If significant amounts of CH are destroyed through this reaction, our conclusion about the importance of non-equilibrium chemistry would be strengthened.

6. Nonthermal Chemistry in Diffuse Clouds

We used the chemical model of Federman et al. (1996a) to examine the effects of non-thermal motions on diffuse cloud chemistry. The origin of the nonthermal motion is assumed to be the result of the propagation of Alfvén waves, constantly entering the cloud from the intercloud medium. The dissipation of these waves is concentrated primarily in a diffuse cloud boundary layer, the transition zone between the cloud and the intercloud medium. The molecular abundances resulting from the Alfvénic driven nonthermal chemistry are calculated for this boundary layer, without considering any time dependence or attempting to describe any changes in physical or chemical conditions throughout the region. Instead, we impose a set of conditions for the clouds toward our sample of stars that are inferred from previous observations or are from the excitation analysis of neutral carbon.

In the chemical model we use a set of 16 atomic and molecular species closely related to CH^+ chemistry. These are H , He , C , O , He^+ , C^+ , H_2 , CO , CH , OH , H_2O , CO^+ , CH^+ , CH_2^+ , CH_3^+ , and HCO^+ . The set of molecules and chemical reactions was chosen so that it constitutes a closed system with reasonable assumptions on the physical conditions in diffuse clouds. The chemical reactions involved in this model are given in Table 8; the rate coefficients were taken from Federman et al. (1997) and Draine & Katz (1986), updated with information from van Dishoeck & Black (1988), Federman & Huntress (1989), Mitchell (1990), Anicich (1993), Millar, Farquhar, & Willacy (1997), and Pan et al. (2001). For example, the CO photodissociation rates come from the tabulation in van Dishoeck & Black (1988) using the observed column densities of CO and H_2 and τ_{UV} . The photodissociation rates for the other molecules included grain attenuation through the τ_{UV} values listed in

Table 7. Abundances of CH, CO, CO⁺, HCO⁺, He⁺, CH₂⁺, and CH₃⁺ were calculated by solving a system of nonlinear rate equations. We assumed that for all lines of sight the He, OH, and H₂O fractional abundances are 0.1, 1.6×10^{-10} , and 3.2×10^{-11} , respectively, based on the theoretical results of Federman et al. (1996b). The abundances of the remaining elements and molecular species, listed in Table 7, were taken from observations (see Section 5) and were kept fixed throughout the analysis. Fractional abundances of neutral carbon are from the present analysis. The electron densities were derived from the C⁺ abundances.

We define an effective temperature for each ion-neutral (and in some cases for each neutral-neutral) reaction in order to introduce the effects of nonthermal motions. Federman et al. (1996a) defined T_{eff} as

$$\frac{3}{2}kT_{eff} = \frac{3}{2}kT + \frac{1}{2}\mu v_{particle}^2. \quad (9)$$

where k and μ are the Boltzmann constant and the reduced mass of the system, respectively. The term $v_{particle}$ is the turbulent velocity of either the ionic (v_{ion}) or the neutral ($v_{neutral}$) species and defined by the root mean square Alfvén wave amplitude or zero, depending on the physical environment we attempted to model.

First, we tested our code by attempting to reproduce the results of Federman et al. (1996a). They imposed a set of conditions on their model clouds that are believed to be representative of the region in which the effects of nonthermal chemistry are significant. Therefore, we modeled their “hypothetical” cloud with fractional abundances of 0.2, 0.076, 2×10^{-4} , 7.94×10^{-5} , and 3.02×10^{-4} for H₂, He, C⁺, N, and O, respectively. The visual extinction was set to 0.3 mag, representative of a predominantly atomic diffuse cloud, corresponding to a value of 0.6 for τ_{UV} . Since we did not calculate CH⁺ abundances, as opposed to Federman et al. (1996a), we used their result for CH⁺ to calculate the amounts of CO⁺, HCO⁺, and CH produced by the nonthermal chemistry. The gas density, temperature, and v_{ion} combinations used for the modeling correspond to their models 1, 2 and 3 – (100 cm⁻³, 100 K, 3 km s⁻¹), (50 cm⁻³, 100 K, 3 km s⁻¹), and (200 cm⁻³, 100 K, 3 km s⁻¹), respectively. In all cases the calculated CO⁺, HCO⁺, and CH abundances were within 30–40% of the values listed in Table 1 of Federman et al. (1996a).

In the models of Federman et al. (1996a), the nonthermal effects were considered only for charged species, reflecting the distinction that ions are tied to the magnetic field. However, if one considers the conservation of momentum during a chemical reaction, then it is plausible that the product species (ion or neutral) could carry some of the momentum from the parent molecules (Gredel et al. 1993; Bucher & Glinski 1999). This would mean that even neutral species, directly produced by reactions involving ionic species, can have more turbulent velocity than the average value for neutrals (not related directly to the ionic species). One

could establish a complex model, where the turbulent velocity progressively decreases from the value representative for ions to that of the average for neutrals, following the chain of chemical reactions from ionic to neutral species. Such an approach is beyond the scope of this study. Instead, we simply explored the phenomena by setting the turbulent velocity for neutral molecules either to the ionic turbulent velocity or zero.

In our approach, we modeled three different situations, one with no turbulence at all (e.g. equilibrium chemistry), one with $v_{ion} \neq 0$ but $v_{neutral} = 0$, and one with nonzero v_{ion} and $v_{neutral} = v_{ion}$. We used the equilibrium CH^+ abundance of 3.3×10^{-12} calculated by Federman et al. (1996a) whenever we attempted to model equilibrium chemistry without any turbulence. Since the observed CH^+ abundance is primarily the product of non-equilibrium chemistry, we would introduce the effects of this chemistry into our “equilibrium” run ($v_{ion} = 0$ and $v_{neutral} = 0$) by using the observed amount of CH^+ . However, we used the observed amount of CH^+ in the cases when the turbulent velocities were set to nonzero. The values for turbulent velocity were chosen to be the amplitude of Alfvénic waves. We adopted a standard value of 3 km s^{-1} for both v_{ion} and $v_{neutral}$ (whenever they differ from zero), following Federman et al. (1996a), based on the typical width of CH^+ absorption lines. We used the temperature and density from the C I excitation analysis (see Table 5) as T and n .

The results of our calculations are shown in Tables 9 and 10 for CH and CO. It is immediately obvious that the observed abundances cannot be reproduced by equilibrium chemistry alone; there are several orders of magnitude difference between the observed and calculated abundances for all lines of sight for both CH and CO. Our results indicate that a nonthermal chemical model for ionic species only produces too much CH. When we also take nonthermal effects into account for neutral–neutral reactions, the observed CH abundances are reproduced reasonably well. The lone exception is the unusual line of sight toward 23 Ori, which has detectable amounts of CH and CH^+ even though the H_2 column is about 10^{18} cm^{-2} . When T_{eff} increases, reaction 17 (see Table 8) becomes more effective in destroying CH. This reaction also increases the amount of CO between models 2 and 3. Unlike the situation for CH, we did not find reasonable agreement for CO in general, indicating the limits of our approximations. The closest correspondence occurs for the denser sight lines, those in Scorpius, suggesting that pockets of higher density control the abundance of CO in diffuse gas. Since a theoretical determination of the rate coefficient for $\text{C}^+ + \text{OH} \rightarrow \text{CO}^+ + \text{H}$ (Dubernet, Gargaud, & McCarroll 1992) suggests a value much larger than that used here, we investigated its affect on CO as well. While the equilibrium abundance for CO increases nearly 5 fold, the non-equilibrium results are changed only 5%. Clearly, the production of CO^+ and HCO^+ , the precursors of CO, is dominated by the presence of enhanced amounts of CH^+ brought about by non-equilibrium chemistry in the sight lines considered here. It is likely that we have to improve our model in other ways as well. For instance, a more precise

description for $v_{neutral}$ is needed as is a more detailed analysis of H₂ and CO photodissociation that includes self- and mutual-shielding.

7. Discussion

Observations and models have suggested long ago that the ISM is not in an equilibrium state. The underlying reason is that interstellar clouds cannot be treated as a closed systems; interactions with often violent surroundings are inevitable. Shock fronts from supernovae and cloud collisions are probably commonplace. These non-equilibrium processes affect the chemistry of most molecular species, including that of CH⁺. In fact, almost everyone agrees that these non-equilibrium processes hold the key for explaining the elusive CH⁺ abundance problem in the ISM. The exact mechanisms and place for CH⁺ production, however, is still the subject of intense debate. MHD shock models (e.g., Flower & Pineau des Forêts 1998) or those that involve intermittent dissipation of interstellar turbulence (e.g., Joulain et al. 1998) suggest that CH⁺ is formed in warm material at temperatures $T > 100$ K. Excitation analysis of interstellar C₂ (Gredel 1999), on the other hand, places the production of CH⁺ into the colder gas at temperatures of 50-100 K. Our results are more consistent with this later suggestion and support the claim that non-equilibrium chemistry is very important (or sometimes even dominant) for CH⁺, CH, and CO in diffuse sight lines. We concur with Gredell (1999) that about 30% of the observed CH is associated with CH⁺ synthesis. The associated molecular ions, CO⁺ and HCO⁺, are likely to be affected as well, with respective abundances reaching $\sim 6 \times 10^{-13}$ and about 5×10^{-11} . (We note in passing that such enhancements in the HCO⁺ abundance still yield column densities at least an order of magnitude below those inferred from absorption of the millimeter-wave continuum from extragalactic sources [Lucas & Liszt 1996]). This conclusion highlights the fact that any model attempting to account for CH⁺ abundances must address the “side-effects” on other species and be able to describe their abundances. Therefore, indirectly, we imposed constraints on the suggested theories thought to be responsible for CH⁺ production in this environment.

There were cases where our simplified models failed, indicating some shortcomings in our approach. It remains to be seen whether the source of these discrepancies is related to the assumed physical environment for particular lines of sight (gradients in physical conditions) or to effects ignored in our approach, such as detailed calculations for H₂ and CO photodissociation. Another possible source of error is the “uniformity” of our approximations. The differences in b -values and Doppler shifts associated with the C I fine structure levels for a given sight line indicate that the levels might not fill the same volume. The excitation

may occur in clumps. A more careful excitation analysis of neutral carbon is necessary to infer average density and temperature for diffuse clouds, but the means to perform such an analysis are beyond the capabilities of current theory and observation. Moreover, we either applied a given turbulence for neutrals or we did not. In reality, the turbulence can change gradually from the values representative for ions to that of neutrals as one follows the chemical network from an ionic parent molecule (like CH^+ in our case) to products (Bucher & Glinski 1999). Further work should explore the importance of these various effects.

8. Summary

We surveyed the physical and chemical conditions in the diffuse ISM with the aim of assessing the importance of non-equilibrium processes. We retrieved a mixture of high and medium resolution spectra from the *HST* archive. The selection criteria for the lines of sight was motivated by the idea to minimize the contribution from the denser diffuse cloud cores, which are satisfactorily described by equilibrium chemistry. We studied transitions involving the fine structure levels of neutral carbon to infer the physical parameters of these clouds through analysis of excitation. Our conclusions can be summarized as follows:

We could identify multiple cloud components along the sight lines for which high-resolution spectra were available and toward HD 112244 where the separation between the components was larger than the resolution of the MR spectra. We derived C I column densities and b -values for the components or provided upper limits for non-detections.

We performed C I excitation analyses for all main components to infer n and T . The gas densities and kinetic temperatures were comparable to the representative values for diffuse clouds.

We calculated the abundances produced by molecular chemistry in the moderately dense regions along our sight lines. By removing the contribution from the molecular chemistry, we quantified the amounts of CH from nonthermal chemistry. Our analysis suggested that the amount of CH associated with CH^+ is at least 30–40% of the amount of CH in general, but in some cases it can reach as high as 90% (e.g., 23 Ori).

Density estimates based on the observed upper limits for C_2 and CN, along with CH columns, and on the assumption that the equilibrium chemistry acts alone were (much) larger than the densities from C I excitation. The discrepancy between these density estimates clearly indicates that the assumption of equilibrium chemistry as the sole contributor is inappropriate.

We modeled the non-equilibrium chemistry related to CH^+ and improved upon the approximation of Federman et al. (1996a) to account for nonthermal motions, the driving force behind non-equilibrium chemistry. We defined effective temperatures for both ions and neutrals which involved thermal and nonthermal motions. We explored the effect of these motions with different combinations of neutral and ion turbulent velocities. We found that the observed amounts of molecular species cannot be reproduced by equilibrium chemistry. Models with non-zero turbulence for ions only also fail; turbulence for both ionic and neutral species was required to match the observations satisfactorily.

In closing, non-equilibrium chemistry is needed to explain the physical and chemical conditions in the diffuse gas toward our sample of stars and substantial amounts of CH are produced by nonthermal chemistry in the diffuse ISM along these sight lines.

A. Appendix

Here we present tables of equivalent widths for C I lines seen in our spectra (Tables 11-19). Comparison is made with other determinations, when available, and with the results of our profile syntheses. The agreement among the various measures is quite good, especially when one considers the fact that the MR spectra from *HST* and the *Copernicus* spectra do not always resolve blended lines or velocity components. Specific examples are given in the notes to each table.

We thank Dan Welty for his comments on the Ph.D. Dissertation from the Univ. of Toledo on which this paper is based. Comments by the anonymous referee improved several points in our paper. This research was supported by STScI grant AR-08352.01-97A. For the *Copernicus* data, we utilized the archive developed by George Sonneborn and available at the Multiwavelength Archive at STScI. We made use of the Simbad database, operated at Centre de Données Astronomiques de Strasbourg, Strasbourg, France.

Table 1. Data for Target Stars

HD	Star	Galactic Coordinates		Distance (pc)	Spectral type	V (mag)	$E(B - V)$ (mag)
		l ($^{\circ}$)	b ($^{\circ}$)				
23630	η Tau	166.67	-23.46	113	B7IIIe	2.87	0.00
24760	ϵ Per	157.35	-10.09	165	B0.5V	2.90	0.09
36861	λ Ori	195.05	-12.00	...	O8III	3.30	0.12
112244	...	303.55	6.03	578	O9Ibe	5.32	0.34
141637	1 Sco	346.10	21.71	160	B1.5Vn	4.64	0.20
143018	π Sco	347.21	20.23	141	B1V	2.89	0.08
143275	δ Sco	350.10	22.49	123	B0.2IVe	2.29	0.16
144470	ω^1 Sco	352.75	22.77	130	B1V	3.95	0.22
147165	σ Sco	351.31	17.00	225	B1III	2.91	0.38

Table 2. *HST* Observations for Our Sight Lines

Star	Dataset
η Tau	z1bw020st,z1bw020tt,z1bw020ut,z1bw020vt,z1bw020wt, z1bw020yt,z1bw0210t
ϵ Per	z2c20206t,z2c20207t,z2c20208t
λ Ori	z3di0204t,z3di0205t,z2c20306t,z2c20307t,z2c20308t, z2520306t,z2520307t,z2520308t
HD 112244	z0yv0506m,z0yv050gt,z0yv060em
1 Sco	z2zx020bp,z2zx020fp,z0zi0708m,z0zi070bm,z0zi070ct, z0zi070dt,z0zi070gt,z0zi070it
π Sco	z0zi0408t,z0zi0409t,z0zi040at,z0zi040bt,z0zi040ct, z0xz0308t,z0xz0309t,z0xz030at,z0zi040et,z0zi040gt
δ Sco	z3di0504t,z3di0505t,z34r020dt,z34r020et,z2c20506t, z2c20507t,z2c20508t
ω^1 Sco	z2c20606t,z2c20607t,z2c20608t
σ Sco	z34r0409t,z13v0108m,z13v0109m,z13v010bm,z13v010cm, z13v010dm,z13v010gm

Table 3. Derived Parameter Values

Star Level	Component A		Component B		
	Column density (cm^{-2})	b -value (km s^{-1})	Doppler shift ^a (km s^{-1})	Column density (cm^{-2})	b -value (km s^{-1})
η Tau					
0	$2.4(\pm 0.2) \times 10^{13}$	2.5 ± 0.3
1	$\leq 7.7 \times 10^{11}$
2	$\leq 5.2 \times 10^{11}$
ϵ Per					
0	$4.4(\pm 0.4) \times 10^{13}$	3.0^b
1	$6.4(\pm 0.6) \times 10^{12}$	2.1 ± 0.2
2	$\leq 8.2 \times 10^{11}$
λ Ori					
0	$1.3(\pm 0.1) \times 10^{14}$	3.0 ± 0.3	-12.1^b	$9.6(\pm 1.0) \times 10^{12}$	3.0^b
1	$5.5(\pm 0.6) \times 10^{13}$	2.4 ± 0.2	-12.1^b	$1.7(\pm 0.2) \times 10^{12}$	3.0^b
2	$9.2(\pm 0.9) \times 10^{12}$	2.5^b	-12.1^b	$1.4(\pm 0.1) \times 10^{12}$	3.0^b
HD 112244					
0	$2.2(\pm 0.2) \times 10^{14}$	4.5 ± 0.5	-23.6 ± 0.2	$1.9(\pm 0.2) \times 10^{14}$	4.0 ± 0.4
1	$3.2(\pm 0.3) \times 10^{13}$	2.2 ± 0.2	-24.1 ± 1.7	$3.2(\pm 0.3) \times 10^{13}$	2.7 ± 0.3
2	$4.4(\pm 0.4) \times 10^{12}$	2.0^b	-23.0^b	$6.4(\pm 0.6) \times 10^{12}$	2.0^b
π Sco					
0	$9.2(\pm 0.9) \times 10^{12}$	4.4 ± 0.4
1	$1.4(\pm 0.1) \times 10^{12}$	2.0^b
2	$\leq 2.4 \times 10^{11}$
1 Sco					
0	$2.5(\pm 0.3) \times 10^{13}$	1.8 ± 0.2	-7.1^b	$2.2(\pm 0.2) \times 10^{13}$	3.1 ± 0.3
1	$3.3(\pm 0.3) \times 10^{13}$	1.5 ± 0.2	-7.1^b	$4.3(\pm 0.4) \times 10^{12}$	2.5 ± 0.3
2	$1.6(\pm 0.2) \times 10^{13}$	1.2 ± 0.1	-7.1^b	$4.0(\pm 0.4) \times 10^{11}$	2.5^b
δ Sco					
0	$8.9(\pm 0.9) \times 10^{13}$	2.3 ± 0.2	-4.8^b	$1.3(\pm 0.1) \times 10^{13}$	1.4 ± 0.1
1	$5.8(\pm 0.6) \times 10^{13}$	1.2 ± 0.1	-4.8^b	$3.8(\pm 0.4) \times 10^{12}$	1.5^b
2	$1.2(\pm 0.1) \times 10^{13}$	1.2 ± 0.1	...	$\leq 6.7 \times 10^{11}$...

Table 3—Continued

Star Level	Component A		Component B		
	Column density (cm^{-2})	b -value (km s^{-1})	Doppler shift ^a (km s^{-1})	Column density (cm^{-2})	b -value (km s^{-1})
ω^1 Sco					
0	$1.6(\pm 0.2) \times 10^{14}$	3.0^b
1	$5.3(\pm 0.5) \times 10^{13}$	1.0^b
2	$1.0(\pm 0.1) \times 10^{13}$	1.0^b
σ Sco					
0	$1.1(\pm 0.1) \times 10^{14}$	2.7 ± 0.3	-9.0 ± 0.1	$8.4(\pm 0.8) \times 10^{12}$	4.0 ± 0.4
1	$9.9(\pm 1.0) \times 10^{13}$	1.8 ± 0.2	...	$\leq 2.1 \times 10^{12}$...
2	$2.5(\pm 0.3) \times 10^{13}$	1.4 ± 0.1	...	$\leq 1.2 \times 10^{12}$...

^a The quantity “Doppler shift” is a shift relative to Component A. It was measured in HR (FWHM $\approx 3 \text{ km s}^{-1}$) spectra and was sometimes adjusted during profile synthesis to improve the fit. In the case of HD 112244, the large shift between the two component could be measured in MR (FWHM $\approx 15 \text{ km s}^{-1}$) spectra.

^b The parameter was kept fixed during the fitting procedure.

Table 4. Collisional deexcitation coefficients

Coeff. ($\text{cm}^3 \text{ s}^{-1}$)	Transition from level i to level j			Notes
	$J=2 \rightarrow 0$	$J=2 \rightarrow 1$	$J=1 \rightarrow 0$	
$\gamma_{i,j}^H$	$7.244 \cdot 10^{-11} T^{0.069}$	$1.413 \cdot 10^{-10} T^{0.156}$	$1.349 \cdot 10^{-10} T^{0.043}$	1
$\gamma_{i,j}^{He}$	$1.995 \cdot 10^{-11} T^{0.181}$	$2.951 \cdot 10^{-11} T^{0.241}$	≈ 0	2,3
$\gamma_{i,j}^{ortho-H_2}$	$3.311 \cdot 10^{-11} T^{0.16}$	$4.365 \cdot 10^{-11} T^{0.27}$	$8.511 \cdot 10^{-11} T^{-0.03}$	4
$\gamma_{i,j}^{para-H_2}$	$1.072 \cdot 10^{-10} T^{-0.04}$	$1.479 \cdot 10^{-10} T^{0.05}$	$1.122 \cdot 10^{-10} T^{-0.10}$	4

The quantity T is the gas temperature.

Notes. – (1) Launay & Roueff 1977; (2) Lavendy et al. 1991; (3) Staemmler & Flower 1991; (4) Schröder et al. 1991.

Table 5. Gas Densities and Temperatures

Star	$n_C I^a$ (cm^{-3})	$T_{H_2}^b$ (K)	n^c (cm^{-3})
η Tau	≤ 3.5	59–143	...
ϵ Per	11.5–33	51–188	...
λ Ori	68–182	36–60	...
HD 112244 A ^d	14–28	67–113	≤ 960
HD 112244 B ^d	16.5–48	67–113	≤ 960
1 Sco	200–800	53–114	≤ 2299
π Sco	13–33	56–144	≤ 2793
δ Sco	90–265	42–81	≤ 1115
ω^1 Sco	43–83	59–94	≤ 643
σ Sco	137–345	50–87	≤ 371
23 Ori	7.5–23	65–150	≤ 4004
β^1 Sco	35–205	77–103	≤ 770

^a Density inferred from the C I level populations.

^b H₂ excitation temperatures of Savage et al. 1977.

^c Density calculated by inverting eqn. 6.

^d A is the stronger and B is weaker component.

Table 6. Chemical Network for the Equilibrium Chemistry

Reaction	Rate coefficient or Rate	Value	Notes
$C^+ + H_2 \rightarrow CH_2^+ + h\nu$	k_1	$1.0 \times 10^{-16} \text{ cm}^3 \text{ s}^{-1}$	1
$C^+ + CH \rightarrow C_2^+ + H$	k_2	$5.4 \times 10^{-10} \text{ cm}^3 \text{ s}^{-1}$	2
$C_2 + N \rightarrow CN + C$	k_3	$1.7 \times 10^{-11} \sqrt{\frac{T}{300}} \text{ cm}^3 \text{ s}^{-1}$	3
$CH + N \rightarrow CN + H$	k_4	$2.0 \times 10^{-11} \sqrt{\frac{T}{300}} \text{ cm}^3 \text{ s}^{-1}$	4
$C^+ + NH \rightarrow \begin{cases} CN^+ + H \\ CH^+ + N \end{cases}$	k_5	$5.0 \times 10^{-10} \text{ cm}^3 \text{ s}^{-1}$	3
$CH + h\nu \rightarrow C + H$	$G(CH)$	$1.3 \times 10^{-9} e^{-\tau_{UV}} \text{ s}^{-1}$	2
$C_2 + h\nu \rightarrow 2C$	$G(C_2)$	$2.0 \times 10^{-10} e^{-\tau_{UV}} \text{ s}^{-1}$	5
$CN + h\nu \rightarrow C + N$	$G(CN)$	$1.0 \times 10^{-10} e^{-\tau_{UV}} \text{ s}^{-1}$	6

Notes.– (1) Federman et al. 1997; (2) Pan et al. 2001; (3) Federman et al. 1994; (4) Messing et al. 1981; (5) Pouilly et al. 1983; (6) Lavendy et al. 1987.

Table 7. Fractional Abundances

Star	τ_{UV}	N_{total}^b	$x(Y)^a$									
			C ⁺	C	N	O	H ₂	CH ⁺	CO	CH	C ₂	CN
η Tau	0.00	2.7(20) ^c	1.4(-4)	9.1(-8)	7.5(-5)	4.0(-4)	2.6(-1)	7.0(-9)	$\leq 8.1(-9)$
ϵ Per	0.56	3.2(20)	1.4(-4)	1.5(-7)	3.2(-5)	3.0(-4)	2.1(-1)	$\leq 3.4(-9)$	2.7(-9)	6.2(-9)
λ Ori	0.74	6.3(20)	1.3(-4)	3.2(-7)	7.9(-5)	3.2(-4)	4.0(-2)	$\leq 1.1(-9)$	6.2(-9)
HD 112244 A	1.05	7.5(20)	1.4(-4)	3.8(-7)	7.5(-5)	4.0(-4)	1.9(-1)	1.0(-8)	1.8(-8)	4.0(-9)	...	$\leq 4.2(-10)$
HD 112244 B	1.05	7.5(20)	1.4(-4)	3.0(-7)	7.5(-5)	4.0(-4)	1.9(-1)	$\leq 3.0(-9)$	5.1(-9)	2.8(-9)	...	$\leq 4.2(-10)$
1 Sco	0.87	1.6(21)	1.6(-4)	6.4(-8)	1.0(-4)	3.5(-4)	2.0(-2)	$\leq 8.8(-10)$	$\leq 1.6(-9)$	$\leq 1.1(-9)$...	$\leq 2.4(-10)$
π Sco	0.35	5.6(20)	1.4(-4)	1.9(-8)	7.5(-5)	3.5(-4)	7.0(-2)	$\leq 2.0(-9)$	1.5(-9)	$\leq 8.9(-10)$	$\leq 3.0(-9)$...
δ Sco	0.69	1.4(21)	1.8(-4)	1.2(-7)	9.8(-5)	4.2(-4)	4.0(-2)	2.4(-9)	2.2(-9)	1.6(-9)	...	$\leq 9.3(-11)$
ω^1 Sco	0.96	1.7(21)	1.4(-4)	1.3(-7)	1.2(-4)	4.3(-4)	1.3(-1)	3.6(-9)	5.3(-9)	1.9(-9)	$\leq 1.0(-9)$...
σ Sco	1.65	2.3(21)	1.4(-4)	1.0(-7)	1.0(-4)	4.3(-4)	5.0(-2)	2.5(-9)	1.3(-9)	1.3(-9)	...	$\leq 5.7(-11)$
23 Ori	0.68	5.5(20)	2.8(-4)	1.7(-6)	8.0(-5)	3.6(-4)	1.0(-2)	2.4(-8)	...	9.3(-9)	...	$\leq 6.7(-10)$
β^1 Sco	0.87	1.4(21)	1.4(-4)	1.0(-7)	6.5(-5)	2.8(-4)	1.0(-1)	4.2(-9)	3.1(-9)	1.5(-9)	$\leq 9.2(-10)$	$\leq 1.0(-10)$

^a Fractional abundance of species Y.

^b $N_{total} = N(\text{H I}) + 2N(\text{H}_2)$.

^c 2.7(20) = 2.7×10^{20} .

Table 8. Chemical Network

Reaction	Rate coefficient or Rate	Notes
1. $\text{CO}^+ + \text{H} \rightarrow \text{CO} + \text{H}^+$	$7.5 \times 10^{-10} \text{ cm}^3 \text{ s}^{-1}$	1
2. $\text{HCO}^+ + \text{e}^- \rightarrow \text{CO} + \text{H}$	$2.4 \times 10^{-7} \times \left(\frac{300}{T_{eff}}\right)^{0.69} \text{ cm}^3 \text{ s}^{-1}$	2
3. $\text{CO} + \text{He}^+ \rightarrow \text{C}^+ + \text{O} + \text{He}$	$1.6 \times 10^{-9} \text{ cm}^3 \text{ s}^{-1}$	1
4. $\text{CO} + \text{h } \nu \rightarrow \text{C} + \text{O}$	$G(\text{CO})^a \text{ s}^{-1}$...
5. $\text{CH}^+ + \text{O} \rightarrow \text{CO}^+ + \text{H}$	$3.5 \times 10^{-10} \text{ cm}^3 \text{ s}^{-1}$	3
6. $\text{CO}^+ + \text{H}_2 \rightarrow \text{HCO}^+ + \text{H}$	$1.4 \times 10^{-9} \text{ cm}^3 \text{ s}^{-1}$	3
7. $\text{CO}^+ + \text{e}^- \rightarrow \text{C} + \text{O}$	$1.0 \times 10^{-7} \times \left(\frac{300}{T_{eff}}\right)^{0.46} \text{ cm}^3 \text{ s}^{-1}$	2
8. $\text{H}_2 + \text{He}^+ \rightarrow \text{He} + \text{H}_2^+$	$1.0 \times 10^{-13} \text{ cm}^3 \text{ s}^{-1}$	3
9. $\text{He} + \text{CR} \rightarrow \text{He}^+ + \text{e}^-$	$1.1/n \times 10^{-17} \text{ cm}^3 \text{ s}^{-1}$	1
10. $\text{He}^+ + \text{e}^- \rightarrow \text{He} + \text{h } \nu$	$2.4 \times 10^{-12} \times \left(\frac{300}{T_{eff}}\right)^{0.64} \text{ cm}^3 \text{ s}^{-1}$	4
11. $\text{CH}_2^+ + \text{e}^- \rightarrow \text{CH} + \text{H}$	$1.25 \times 10^{-7} \times \sqrt{\frac{300}{T_{eff}}} \text{ cm}^3 \text{ s}^{-1}$	2
12. $\text{CH}_3^+ + \text{e}^- \rightarrow \text{CH} + \text{H}_2$	$2.45 \times 10^{-7} \times \sqrt{\frac{300}{T_{eff}}} \text{ cm}^3 \text{ s}^{-1}$	2
13. $\text{C} + \text{H} \rightarrow \text{CH} + \text{h } \nu$	$1.0 \times 10^{-17} \text{ cm}^3 \text{ s}^{-1}$	4
14. $\text{C}^+ + \text{CH} \rightarrow \text{CH}^+ + \text{C}$	$1.5 \times 10^{-9} \text{ cm}^3 \text{ s}^{-1}$	5,6
15. $\text{C}^+ + \text{CH} \rightarrow \text{C}_2^+ + \text{H}$	$5.4 \times 10^{-10} \text{ cm}^3 \text{ s}^{-1}$	5,6
16. $\text{C} + \text{CH} \rightarrow \text{C}_2 + \text{H}$	$1.0 \times 10^{-12} \times \sqrt{T_{eff}} \text{ cm}^3 \text{ s}^{-1}$	1
17. $\text{CH} + \text{O} \rightarrow \text{CO} + \text{H}$	$9.5 \times 10^{-11} \times \sqrt{\frac{T_{eff}}{300}} \text{ cm}^3 \text{ s}^{-1}$	5
18. $\text{CH} + \text{h } \nu \rightarrow \text{CH}^+ + \text{e}^-$	$4.2 \times 10^{-10} \times \text{e}^{-\tau_{UV}} \text{ s}^{-1}$	7
19. $\text{CH} + \text{h } \nu \rightarrow \text{C} + \text{H}$	$1.3 \times 10^{-9} \times \text{e}^{-\tau_{UV}} \text{ s}^{-1}$	8
20. $\text{CH}^+ + \text{H}_2 \rightarrow \text{CH}_2^+ + \text{H}$	$1.2 \times 10^{-9} \text{ cm}^3 \text{ s}^{-1}$	1
21. $\text{CH}_2^+ + \text{H}_2 \rightarrow \text{CH}_3^+ + \text{H}$	$1.2 \times 10^{-9} \text{ cm}^3 \text{ s}^{-1}$	3
22. $\text{CH}_2^+ + \text{O} \rightarrow \text{HCO}^+ + \text{H}$	$7.5 \times 10^{-10} \text{ cm}^3 \text{ s}^{-1}$	1
23. $\text{CH}_2^+ + \text{e}^- \rightarrow \text{C} + \text{H}_2$	$1.25 \times 10^{-7} \times \sqrt{\frac{300}{T_{eff}}} \text{ cm}^3 \text{ s}^{-1}$	2
24. $\text{CH}_3^+ + \text{O} \rightarrow \text{HCO}^+ + \text{H}_2$	$4.40 \times 10^{-10} \text{ cm}^3 \text{ s}^{-1}$	3
25. $\text{CH}_3^+ + \text{e}^- \rightarrow \text{CH}_2 + \text{H}$	$7.0 \times 10^{-8} \times \sqrt{\frac{300}{T_{eff}}} \text{ cm}^3 \text{ s}^{-1}$	2
26. $\text{CH}_3^+ + \text{e}^- \rightarrow \text{C} + \text{H}_2 + \text{H}$	$3.5 \times 10^{-8} \times \sqrt{\frac{300}{T_{eff}}} \text{ cm}^3 \text{ s}^{-1}$	2
27. $\text{C}^+ + \text{H}_2 \rightarrow \text{CH}_2^+ + \text{h } \nu$	$1.0 \times 10^{-16} \text{ cm}^3 \text{ s}^{-1}$	8
28. $\text{C}^+ + \text{OH} \rightarrow \text{CO}^+ + \text{H}$	$7.7 \times 10^{-10} \text{ cm}^3 \text{ s}^{-1}$	4
29. $\text{C}^+ + \text{H}_2\text{O} \rightarrow \text{HCO}^+ + \text{H}$	$9.0 \times 10^{-10} \text{ cm}^3 \text{ s}^{-1}$	4
30. $\text{CH} + \text{H} \rightarrow \text{C} + \text{H}_2$	$5.0 \times 10^{-11} \times \sqrt{\frac{T_{eff}}{300}} \text{ cm}^3 \text{ s}^{-1}$	4

Notes. – (1) Draine & Katz 1986; (2) Mitchell 1990; (3) Anicich 1993; (4) Millar et al. 1997; (5) Federman & Huntress 1989; (6) Pan et al. 2001; (7) Barsuhn & Nesbit 1978; (8) Federman et al. 1997.

^a $G(\text{CO})$ in units of 10^{-10} s^{-1} are 1.6, 1.3, 1.2, 1.1, 1.1, 1.2, 1.4, 1.3, 1.1, 0.89, 1.6, and 1.1 for η Tau, ϵ Per, λ Ori, HD 112244 A, HD 112244 B, 1 Sco, π Sco, δ Sco, ω^1 Sco, σ Sco, 23 Ori, and β^1 Sco, respectively.

Table 9. CH Fractional Abundances

Star	Observed ^a	Model 1 ^b	Model 2 ^c	Model 3 ^d
η Tau	...	$\leq 6.1 \times 10^{-12}$	$\leq 2.8 \times 10^{-9}$	$\leq 2.7 \times 10^{-9}$
ϵ Per	$\leq 6.2 \times 10^{-9}$	$(2.2-5.3) \times 10^{-11}$	$(0.5-1.2) \times 10^{-8}$	$(4.2-7.4) \times 10^{-9}$
λ Ori	...	$(1.2-1.8) \times 10^{-11}$	$(0.9-1.4) \times 10^{-9}$	$(4.6-5.2) \times 10^{-10}$
HD 112244 A	4.0×10^{-9}	$(3.3-5.4) \times 10^{-11}$	$(2.2-3.6) \times 10^{-8}$	$(1.6-2.2) \times 10^{-8}$
HD 112244 B	2.8×10^{-9}	$(3.6-6.9) \times 10^{-11}$	$(0.7-1.4) \times 10^{-8}$	$(5.2-7.4) \times 10^{-9}$
1 Sco	$\leq 1.1 \times 10^{-9}$	$(6.5-9.9) \times 10^{-12}$	$(3.5-5.3) \times 10^{-10}$	$(1.8-2.0) \times 10^{-10}$
π Sco	$\leq 8.9 \times 10^{-10}$	$(0.6-1.3) \times 10^{-11}$	$(0.8-1.8) \times 10^{-9}$	$(0.7-1.1) \times 10^{-9}$
δ Sco	1.6×10^{-9}	$(1.4-2.3) \times 10^{-11}$	$(1.9-3.0) \times 10^{-9}$	$(1.0-1.1) \times 10^{-9}$
ω^1 Sco	1.9×10^{-9}	$(3.7-5.4) \times 10^{-11}$	$(0.9-1.3) \times 10^{-8}$	$(5.3-6.1) \times 10^{-9}$
σ Sco	1.3×10^{-9}	$(1.9-2.5) \times 10^{-11}$	$(3.2-4.2) \times 10^{-9}$	$(1.5-1.6) \times 10^{-9}$
23 Ori	9.3×10^{-9}	$(1.2-2.9) \times 10^{-12}$	$(1.0-2.4) \times 10^{-9}$	$(0.8-1.5) \times 10^{-9}$
β^1 Sco	1.5×10^{-9}	$(2.4-4.2) \times 10^{-11}$	$(0.7-1.2) \times 10^{-8}$	$(4.2-5.6) \times 10^{-9}$

^a References – Federman 1982; Danks et al. 1984; Federman et al. 1997.

^b Equilibrium chemistry ($v_{ion} = 0$, $v_{neutral} = 0$, $x(\text{CH}^+) = 3.3 \times 10^{-12}$).

^c Non-equilibrium chemistry ($v_{ion} = 3 \text{ km s}^{-1}$, $v_{neutral} = 0$, observed $x(\text{CH}^+)$).

^d Non-equilibrium chemistry ($v_{ion} = 3 \text{ km s}^{-1}$, $v_{neutral} = 3 \text{ km s}^{-1}$, observed $x(\text{CH}^+)$).

Table 10. CO Fractional Abundances

Star	Observed ^a	Model 1 ^b	Model 2 ^c	Model 3 ^d
η Tau	$\leq 8.1 \times 10^{-9}$	$\leq 7.7 \times 10^{-13}$	$\leq 1.6 \times 10^{-10}$	$\leq 1.7 \times 10^{-10}$
ϵ Per	2.7×10^{-9}	$(2.8-6.9) \times 10^{-12}$	$(2.4-4.6) \times 10^{-10}$	$(2.6-5.8) \times 10^{-10}$
λ Ori	6.2×10^{-9}	$(1.2-3.2) \times 10^{-11}$	$(1.6-4.0) \times 10^{-10}$	$(1.8-4.4) \times 10^{-10}$
HD 112244 A	1.8×10^{-8}	$(4.0-7.6) \times 10^{-12}$	$(1.1-1.8) \times 10^{-9}$	$(1.2-2.3) \times 10^{-9}$
HD 112244 B	5.1×10^{-9}	$(0.5-1.3) \times 10^{-11}$	$(3.8-9.8) \times 10^{-10}$	$(0.4-1.2) \times 10^{-9}$
1 Sco	$\leq 1.6 \times 10^{-9}$	$(0.4-1.7) \times 10^{-10}$	$(0.3-1.2) \times 10^{-9}$	$(0.4-1.3) \times 10^{-9}$
π Sco	1.5×10^{-9}	$(2.4-5.7) \times 10^{-12}$	$(0.8-1.6) \times 10^{-10}$	$(0.8-1.8) \times 10^{-10}$
δ Sco	2.2×10^{-9}	$(2.1-5.9) \times 10^{-11}$	$(0.5-1.3) \times 10^{-9}$	$(0.6-1.5) \times 10^{-9}$
ω^1 Sco	5.3×10^{-9}	$(1.1-2.1) \times 10^{-11}$	$(1.0-1.7) \times 10^{-9}$	$(1.1-2.0) \times 10^{-9}$
σ Sco	1.3×10^{-9}	$(3.8-9.3) \times 10^{-11}$	$(1.5-3.4) \times 10^{-9}$	$(1.7-3.9) \times 10^{-9}$
23 Ori	...	$(2.0-5.9) \times 10^{-12}$	$(1.7-4.9) \times 10^{-10}$	$(1.7-5.0) \times 10^{-10}$
β^1 Sco	3.1×10^{-9}	$(0.8-4.7) \times 10^{-11}$	$(0.5-2.9) \times 10^{-9}$	$(0.6-3.4) \times 10^{-9}$

^a Crenny & Federman, private communication.

^b Equilibrium chemistry ($v_{ion} = 0$, $v_{neutral} = 0$, $x(\text{CH}^+) = 3.3 \times 10^{-12}$).

^c Non-equilibrium chemistry ($v_{ion} = 3 \text{ km s}^{-1}$, $v_{neutral} = 0$, observed $x(\text{CH}^+)$).

^d Non-equilibrium chemistry ($v_{ion} = 3 \text{ km s}^{-1}$, $v_{neutral} = 3 \text{ km s}^{-1}$, observed $x(\text{CH}^+)$).

Table 11. W_λ (mÅ) of C I Lines toward η Tau

Wavelength (Å)	Measured	Calculated
J = 0:		
1260.736	8.39 ± 1.51	10.64
1277.245	16.38 ± 1.24	19.88
1280.135	7.30 ± 1.09	7.38
1328.833	16.59 ± 0.99	15.46
1560.309	24.72 ± 0.86	24.50
1656.928	33.87 ± 1.06	34.47

Table 12. W_λ (mÅ) of C I Lines toward ϵ Per

λ (Å)	Measured		Previous Measurements		Calculated
	<i>HST</i>	<i>Copernicus</i>	JS ^a	JJL ^b	
J = 0:					
1260.736	18.77 ± 0.34	14.0 ± 0.7	17.32
1328.833	...	22.3 ± 0.6	...	29.0 ± 1.5	24.06
J = 1:					
1260.927	≤ 0.32	≤ 1.3	1.14
1260.996	≤ 0.32	≤ 1.2	0.86
1261.122	≤ 0.32	≤ 1.2	1.42
1329.085	1.84
1329.100	...	5.5 ^c ± 0.6	3.5 ^c ± 1.8	5.4 ^c ± 0.9	2.28
1329.123	1.40
J = 2:					
1261.426	≤ 0.32	≤ 1.4	...
1261.552	≤ 0.32	≤ 1.4	...
1329.578	...	≤ 0.6 ^d	≤ 4.0 ^d	≤ 2.2 ^d	...

^a Jenkins & Shaya 1979.

^b Jenkins et al. 1983.

^c Total W_λ for $\lambda\lambda$ 1329.085, 1329.100, 1329.123.

^d Total W_λ for $\lambda\lambda$ 1329.578, 1329.601.

Table 13. W_λ (mÅ) of C I Lines toward λ Ori

λ (Å)	Measured		Other Measurements		Calculated
	HR ^a	MR ^a	JS ^b	JJL ^c	
J = 0:					
1157.910A ^d	26.97 ± 0.26	28.09
1157.910B ^d	2.59 ± 0.30	4.25
1158.324A	15.28 ± 0.23	15.52
1158.324B	2.99 ± 0.35	1.52
1260.736A	...	35.44 ± 0.33	37.0 ^e ± 2.0	38.0 ^e ± 2.6	31.27
1260.736B	...	3.17 ± 0.24	4.88
1328.833	...	48.23 ± 0.32	52.0 ^e ± 4.0	51.0 ^e ± 2.6	45.66
J = 1:					
1157.770	5.82 ± 0.21	5.58
1158.035	8.95 ± 0.21	9.56
1158.130	4.42 ^f ± 0.21	4.28
1158.674	0.85 ± 0.09	1.25
1158.732	1.39 ± 0.10	1.47
1260.927	...	5.17 ± 0.22	...	≤ 6.3	8.71
1260.996	...	9.55 ± 0.36	...	6.3 ± 2.1	6.84
1261.122	...	9.73 ± 0.30	13.0 ± 1.0	7.6 ± 2.1	10.43
1329.085	12.96
1329.100	...	47.83 ^g ± 0.32	42.0 ^g ± 2.0	56.0 ^g ± 3.0	15.25
1329.123	10.39
J = 2:					
1158.019	2.15 ± 0.21	4.03
1158.132	0.44
1158.397	0.87 ± 0.21	0.74
1261.426	...	1.95 ± 0.29	3.4 ^h ± 1.2	≤ 6.3	1.45
1261.552	...	4.82 ± 0.32	...	≤ 6.6	4.17
1329.578	...	11.68 ⁱ ± 0.32	14.0 ⁱ ± 2.0	9.5 ⁱ ± 3.7	6.60
1329.601	2.34

^a HR: High Resolution spectra, MR: Medium Resolution spectra.

^b Jenkins & Shaya 1979.

^c Jenkins et al. 1983.

^d A: Main component B: Secondary component, if resolved.

^e Involves both the main and secondary $J = 0$ components.

^f Blended with λ 1158.132 ($J = 2$).

^g Total W_λ for $\lambda\lambda$ 1329.085, 1329.100, 1329.123.

^h Total W_λ for $\lambda\lambda$ 1261.426, 1261.552.

ⁱ Total W_λ for $\lambda\lambda$ 1329.578, 1329.601.

Table 14. W_λ (mÅ) of C I Lines toward HD 112244

λ (Å)	Measured		Calculated	
	Component A	Component B	Component A	Component B
J = 0:				
1188.833 ^a	53.66 ± 2.42	32.44 ± 2.05	29.26	25.16
1193.031 ^b	52.65 ± 2.46	47.22 ± 2.51	45.28	39.42
1193.996	22.36 ± 1.91	25.10 ± 2.24	24.77	21.23
1260.736	39.11 ± 1.20	27.60 ± 1.26	48.07	41.85
1276.483	10.16 ± 0.68	14.27 ± 0.98	12.31	10.46
1277.245 ^c	75.27 ± 1.28	63.47 ± 1.16	61.93	54.31
1280.135	44.19 ± 1.40	29.04 ± 1.07	40.22	34.80
1560.309	76.95 ± 2.71	61.83 ± 2.35	75.89	66.56
J = 1:				
1188.993 ^a	13.37 ± 1.77		2.13	2.12
1193.009 ^b	...		9.54	9.90
1193.264	...		4.06	4.08
1193.679	...		3.72	3.73
1260.927	...		5.22	5.26
1260.996	...		4.04	4.05
1261.122	...		6.34	6.44
1277.282 ^c	...		18.42	20.23
1277.513	28.50 ± 0.99		8.92	9.19
1279.890	5.40 ± 1.13	...	5.57	5.63
1560.682 ^d	32.71 ± 2.35	35.82 ± 2.26	22.69	24.95
1560.709 ^d	11.03	11.37
J = 2:				
1193.240	...		1.96	2.81
1193.393	...		0.36	0.53
1193.649	...		0.02	0.04
1261.426	...		0.60	0.87
1261.552	...		1.75	2.52
1277.550	...		4.57	6.38
1277.723	...		0.90	1.31
1561.340 ^e	...		1.12	1.62
1561.438 ^e	17.60 ± 2.21		5.67	7.91

^a Neutral carbon lines are obscured by a strong Cl I.

^b Blended lines. The total W_λ is listed for the stronger line.

^c Blended lines. The total W_λ is listed for the stronger line.

^d Blended lines. The total W_λ is listed for the stronger line.

^e Blended lines. The total W_λ is listed for the stronger line.

Table 15. W_λ (mÅ) of C I Lines toward 1 Sco

λ (Å)	Measured		Other measurement	Calculated
	HR ^a	MR ^a	JJL ^b	
J = 0:				
1193.031A ^c	10.43 ± 0.62	9.35
1193.031B	11.46 ± 0.62	9.56
1193.996A ^d	3.63 ± 0.42	3.62
1193.996B ^d	3.02 ± 0.62	3.37
1260.736	...	19.73 ^e ± 0.98	22.0 ^e ± 2.4	20.18 ^e
1277.245	...	69.20 ^f ± 1.42	...	37.48 ^e
1280.135A	...	7.38 ± 0.70	...	7.11
1280.135B	...	7.06 ± 0.73	...	6.94
1328.833A	12.97 ± 0.66	14.50 ± 0.86	34.0 ^e ± 4.4	13.98
1328.833B	15.82 ± 0.98	14.50 ± 0.85	...	15.23
1560.309A	...	26.72 ± 0.83	...	21.13
1560.309B	...	14.15 ± 0.75	...	25.06
1656.928A	...	37.89 ± 0.97	...	28.11
1656.928B	...	28.58 ± 0.90	...	37.20
J = 1:				
1193.009 ^c	2.89 ± 0.46	10.35
1193.679	4.19 ± 0.52	4.21
1194.406	1.46 ± 0.37	1.67
1260.927	...	5.23 ± 0.94	≤ 6.6	5.85
1260.996	...	3.45 ± 0.78	≤ 6.6	4.57
1261.122	...	5.11 ± 0.81	≤ 6.0	7.05
1277.513 ^g	...	4.75 ± 1.15	...	9.76
1279.890	...	5.56 ± 0.74	...	6.23
1280.597	...	2.20 ± 0.90	...	3.39
1329.085	6.59 ± 0.52	8.82
1329.100	9.26 ± 0.56	26.90 ^h ± 1.10	38.0 ^h ± 3.3	10.47
1329.123	7.05 ± 0.63	7.01
1560.682	...	32.4 ⁱ ± 0.98	...	23.87
1560.709	12.07
1656.267	...	25.89 ± 0.93	...	25.70
1657.379	...	19.09 ± 0.86	...	19.42
1657.907	...	22.75 ± 0.94	...	22.96
J = 2:				
1261.426	...	1.20 ± 0.94	≤ 6.3	2.11
1261.552	...	3.68 ± 0.68	≤ 6.3	5.41

Table 15—Continued

λ (Å)	Measured		Other measurement	Calculated
	HR ^a	MR ^a	JJL ^b	
1277.550 ^g	...	13.07 ± 0.87	...	10.89
1277.723	...	1.80 ± 0.89	...	3.05
1280.333	...	2.50 ± 0.90	...	3.09
1329.578	6.76 ± 0.55	10.30 ^j ± 0.94	≤ 8.7 ^j	7.91
1329.601	4.63 ± 0.72	3.30
1561.340	...	3.26 ± 0.67	...	3.78
1561.438	...	13.08 ± 0.81	...	13.42
1657.008	...	15.43 ± 0.75	...	18.04
1658.121	...	8.99 ± 0.68	...	9.91

^a HR: High Resolution spectra, MR: Medium Resolution spectra.

^b Jenkins et al. 1983.

^c Blended lines.

^d A: Main component B: Secondary component, if resolved.

^e Involves both the main and secondary $J = 0$ components.

^f Involves a second component and $\lambda 1277.282$.

^g Blended lines.

^h Total W_λ for $\lambda\lambda 1329.085, 1329.100, 1329.123$.

ⁱ Total W_λ for $\lambda\lambda 1560.682, 1560.709$.

^j Total W_λ for $\lambda\lambda 1329.578, 1329.601$.

Table 16. W_λ (mÅ) of C I Lines toward π Sco

λ (Å)	Measured	<u>Other Measurement</u> JS ^a	Calculated
J = 0:			
1260.736	3.40 ± 0.95	4.9 ± 2.0	4.84
1277.245 ^b	13.46 ± 0.49	...	11.28
1280.135	2.80 ± 0.50	...	3.14
1328.833	8.97 ± 0.32	...	7.69
1560.309	10.63 ± 0.66	...	13.97
1656.928	26.74 ± 0.74	...	24.74
J = 1:			
1260.927	≤ 0.94	...	0.25
1260.996	≤ 0.94	...	0.19
1261.122	≤ 0.94	≤ 0.7	0.32
1277.282	1.40
1277.513	≤ 0.38	...	0.48
1279.890	≤ 0.50	...	0.27
1280.404	≤ 0.50	...	0.09
1329.085	0.41
1329.100	$1.80^c \pm 0.32$...	0.52
1329.123	0.31
1560.682	$2.17^d \pm 0.64$...	1.73
1560.709	0.59
1656.267	1.92 ± 0.50	...	1.89
1657.379	1.15
1657.907	1.53
J = 2:			
1261.552	≤ 0.94	≤ 0.8	...

^a Jenkins & Shaya 1979.

^b Involves $\lambda 1277.282$.

^c Total W_λ for $\lambda\lambda 1329.085, 1329.100, 1329.123$.

^d Total W_λ for $\lambda\lambda 1560.682, 1560.709$.

Table 17. W_λ (mÅ) of C I Lines toward δ Sco

λ (Å)	Measured		Other measurement	Calculated
	HR ^a	MR ^a	JS ^b	
J = 0:				
1157.910A ^c	23.06 ± 0.28	20.36
1157.910B ^c	2.11 ± 0.20	4.87
1158.324A	10.84 ± 0.23	10.78
1158.324B	1.44 ± 0.25	1.89
1260.736A	21.46 ± 0.43	28.53 ^d ± 0.22	32.0 ^d ± 3.0	22.72
1260.736B	6.03 ± 0.36	5.56
J = 1:				
1157.770	5.06 ± 0.21	5.38
1158.035 ^e	7.98 ± 0.21	8.51
1158.130 ^f	4.05 ± 0.22	4.24
1158.674	1.37 ± 0.14	1.32
1158.732	1.59 ± 0.13	1.53
1260.927	7.63 ± 0.30	8.00 ± 0.20	...	7.99
1260.996	6.54 ± 0.31	6.50 ± 0.19	7.2 ± 1.0	6.49
1261.122	8.15 ± 0.31	8.80 ± 0.21	9.7 ± 2.0	9.27
J = 2:				
1158.019 ^e	4.06 ± 0.26	3.94
1158.132 ^f	0.43 ± 0.22	0.49
1158.397	0.81 ± 0.21	0.81
1158.967	0.45 ± 0.09
1261.426	1.61 ± 0.30	2.74 ± 0.26	...	1.55
1261.552	3.87 ± 0.35	4.95 ± 0.21	4.6 ± 1.4	4.09

^a HR: High Resolution spectra, MR: Medium Resolution spectra.

^b Jenkins & Shaya 1979.

^c A: Main component B: Secondary component, if resolved.

^d Involves both the main and secondary $J = 0$ components.

^e Blended lines.

^f Blended lines.

Table 18. W_λ (mÅ) of C I Lines toward ω^1 Sco

λ (Å)	Measured		Other measurements		Calculated
	<i>HST</i>	<i>Copernicus</i>	SJ ^a	JJL ^b	
J = 0:					
1260.736	35.54 ± 0.14	...	26.0 ± 1.7	33.0 ± 3.6	33.16
1276.483	...	6.6 ± 4.1	...	≤ 6.4	8.85
1328.833	...	22.2 ± 4.1	...	62.0 ± 6.2	39.63
J = 1:					
1260.927	8.19 ± 0.12	...	4.7 ± 1.6	≤ 5.8	6.46
1260.996	6.42 ± 0.11	...	2.7 ± 1.6	≤ 5.7	5.31
1261.122	8.22 ± 0.13	...	11.0 ± 1.7	≤ 5.7	7.41
1329.085	8.80
1329.100	...	$42.5^c \pm 4.1$...	$47.0^c \pm 5.2$	9.81
1329.123	7.49
J = 2:					
1261.426	≤ 3.3	≤ 5.8	1.31
1261.552	4.34 ± 0.14	...	≤ 3.3	≤ 6.6	3.46
1329.578	...	$4.9^d \pm 4.1$...	$\leq 7.1^d$	5.16
1329.601	2.06

^a Snow & Jenkins 1980.

^b Jenkins et al. 1983.

^c Total W_λ for $\lambda\lambda$ 1329.085, 1329.100, 1329.123.

^d Total W_λ for $\lambda\lambda$ 1329.578, 1329.601.

Table 19. W_λ (mÅ) of C I Lines toward σ Sco

λ (Å)	Measured		Other measurement	Calculated
	HR ^a	MR ^a	JS ^b	
J = 0:				
1260.736A ^c	23.59 ± 0.64	36.08 ^d ± 0.50	23.0 ± 2.0	26.59
1260.736B ^c	2.41 ± 0.41	4.40
1328.833	...	50.90 ^d ± 0.50	...	39.57
1560.309	...	56.50 ^d ± 0.54	...	55.97
J = 1:				
1260.927	12.46 ± 0.51	9.40 ± 0.50	...	11.90
1260.996	10.04 ± 0.47	11.10 ± 0.50	...	9.83
1261.122	11.87 ± 0.48	11.84 ± 0.50	14.0 ± 2.0	13.61
1329.085	16.12
1329.100	...	42.80 ^e ± 0.50	...	17.91
1329.123	13.78
1560.682	...	28.60 ± 0.45	...	29.34
1560.709	...	19.10 ± 0.38	...	20.80
J = 2:				
1261.426	...	3.60 ± 0.50	4.3 ± 2.0	3.11
1261.552	...	6.50 ± 0.50	11.5 ± 2.0	7.53
1329.578	...	9.40 ± 0.37	...	10.55
1329.601	...	6.20 ± 0.37	...	4.78
1561.340	...	1.69 ± 0.32	...	5.50
1561.438	...	16.10 ± 0.43	...	16.69

^a HR: High Resolution spectra, MR: Medium Resolution spectra.

^b Jenkins & Shaya 1979.

^c A: Main component B: Secondary component, if resolved.

^d Involves both the main and secondary $J = 0$ components.

^e Total W_λ for $\lambda\lambda$ 1329.085, 1329.100, 1329.123.

REFERENCES

- Allen, M. M., Snow, T. P., & Jenkins, E. B. 1990, *ApJ*, 355, 130
- Anicich, V. G. 1993, *ApJS*, 84, 215
- Barsuhn, J., & Nesbit, R. K. 1978, *J. Chem. Phys.*, 68, 2783
- Bevington, P. R., & Robinson, D. K. 1992, *Data Reduction and Error Analysis for the Physical Sciences*, (Boston: WCB McGraw-Hill)
- Bucher, M. E., & Glinski, R. J. 1999, *MNRAS*, 308, 29
- Charnley, S. B., & Butner, H. 1995, *Ap&SS*, 224, 443
- Crane, P., Lambert, D. L., & Sheffer, Y. 1995, *ApJS*, 99, 107
- Danks, A. C., Federman, S. R., & Lambert, D. L. 1984, *A&A*, 130, 62
- de Geus, E. J. 1992, *A&A*, 262, 258
- de Geus, E. J., Bronfman, L., Thaddeus, P. 1990, *A&A*, 231, 137
- Draine, B. T., & Katz, N. 1986, *ApJ*, 306, 655
- Dubernet, M. L., Gargaud, M., & McCarroll, R. 1992, *A&A*, 259, 373
- Duley, W. W., Hartquist, T. W., Sternberg, A., Wagenblast, R., & Williams, D. A. 1992, *MNRAS*, 255, 463
- Falgarone, E., Pineau des Forêts, G., & Roueff, E. 1995, *A&A*, 300, 870
- Federman, S. R. 1982, *ApJ*, 257, 125
- Federman, S. R., & Huntress, W. T. 1989, *ApJ*, 338, 140
- Federman, S. R., Strom, C. J., Lambert, D. L., Cardelli, J. A., Smith, V. V., Joseph, C. L. 1994, *ApJ*, 424, 772
- Federman, S. R., Rawlings, J. M. C., Taylor, S. D., & Williams, D. A. 1996a, *MNRAS*, 279, L41
- Federman, S. R., Weber, J., & Lambert, D. L., 1996b, *ApJ*, 463, 181
- Federman, S. R., Welty, D. E., & Cardelli, J. A. 1997, *ApJ*, 481, 795

- Federman, S. R., & Zsargó, J. 2001, *ApJ*, 55, 1020
- Flower, D. R., & Pineau des Forêts, G. 1998, *MNRAS*, 297, 1182
- Gredel, R. 1999, *A&A*, 351, 657
- Gredel, R., van Dishoeck, E. F., & Black, J. H. 1993, *A&A*, 269, 477
- Harding, L. B., Guadagnini, R., & Schatz, G. C. 1993, *J. Phys. Chem.*, 97, 5472
- Hobbs, L. M. 1974, *ApJ*, 191, 381
- Hogerheijde, M. R., de Geus, E. J., Spaans, M., van Langevelde, H. J., & van Dishoeck, E. F. 1995, *ApJ*, 441, L93
- Hollenbach, D. J., & Tielens, A. G. G. M. 1999, *RvMP*, 71, 173
- Jenkins, E. B., Jura, M., & Loewenstein, M. 1983, *ApJ*, 270, 88
- Jenkins, E. B., & Shaya, E. J. 1979, *ApJ*, 231, 55
- Joulain, K., Falgarone, E., Pineau des Forêts, G., & Flower, D. 1998, *A&A*, 340, 241
- Kemp, S. N., Bates, B., & Lyons, M. A. 1993, *A&A*, 278, 542
- Krelowski, J., Megier, A., & Strobel, A. 1996, *A&A*, 308, 908
- Lambert, D. L., & Danks, A. C. 1986, *ApJ*, 303, 401
- Lambert, D. L., Sheffer, Y., Gilliland, R. L., & Federman, S. R. 1994, *ApJ*, 420, 756
- Lavendy, H., Robbe, J. M., & Gandara, G. 1987, *J. Phys. B*, 20, 3067
- Lavendy, H., Robbe, J. M., & Roueff, E. 1991, *A&A*, 241, 317
- Launay, J. M., & Roueff, E. 1977, *A&A*, 56, 289
- Lucas, R., & Liszt, H. 1996, *A&A*, 307, 237
- Lugger, P. M., York, D. G., Blanchard, T., & Morton, D. C. 1978, *ApJ*, 224, 1059
- Martin, E. R., & York, D. G. 1982, *ApJ*, 257, 135
- Messing, I., Filseth, S. V., Sadowski, C. M., & Carrington, T. 1981, *J. Chem. Phys.*, 74, 3874
- Meyer, D. M., Jura, M., & Cardelli, J. A. 1998, *ApJ*, 493, 222

- Millar, T. J., Farquhar, P. R. A., & Willacy, K. 1997, *A&AS*, 121, 139
- Mitchell, G. F., & Deveau, T. J. 1983, *ApJ*, 266, 646
- Mitchell, J. B. A. 1990, *Phys. Rep.*, 186, 215
- Morton, D.C. 1991, *ApJS*, 77, 119
- Pan, K., Federman, S. R., & Welty, D. E. 2001, *ApJ*, 558, L105
- Pety, J., & Falgarone, E. 2000, *A&A*, 356, 279
- Pineau des Forêts, G., Flower, D. R., Hartquist, T. W., & Dalgarno, A. 1986, *MNRAS*, 220, 801
- Pouilly, B., Robbe, J. M., Schamps, J., & Roueff, E. 1983, *J. Phys. B*, 16, 437
- Price, R. J., Crawford, I. A., Barlow, M. J., & Howrath, I. D. 2001, *MNRAS*, 328, 555
- Savage, B. D., Bohlin, R. C., Drake, J. F., & Budich, W. 1977, *ApJ*, 216, 291
- Schröder, K., Staemmler, V., Smith, M. D., Flower, D. R., & Jaquet, R. 1991, *J. Phys. B*, 24, 2487
- Snow, T. P., & Jenkins, E. B. 1980, *ApJ*, 241, 161
- Sofia, U. J., Cardelli, J. A., Guerin, K. P., & Meyer, D. M. 1997, *ApJ*, 482, L105
- Staemmler, V., & Flower, D. R. 1991, *J. Phys. B*, 24, 2343
- Trapero, J., Beckman, J. E., Genova, R., & McKeith, C. D. 1992, *ApJ*, 394, 552
- van Dishoeck, E. F., & Black, J. H. 1988, *ApJ*, 334, 771
- van Harrevelt, R., van Hemert, M. C., & Schatz, G. C. 2002, *J. Chem. Phys.*, 116, 6002
- Vidal-Madjar, A., Laurent, C., Ferlet, R., & York, D. G. 1982, *ApJ*, 260, 128
- Welty, D. E., & Hobbs, L. M. 2000, *ApJS*, 133, 345
- Welty, D. E., Hobbs, L. M., & Kulkarni, V. P. 1994, *ApJ*, 436, 152
- White, R. E. 1984, *ApJ*, 284, 685
- York, D. G., Spitzer, L., Jenkins, E. B., Bohlin, R. C., Hill, J., Savage, B. D., & Snow, T. P. 1983, *ApJ*, 266, L55

Zsargó, J., Federman, S. R., & Cardelli, J. A. 1997, *ApJ*, 484, 820

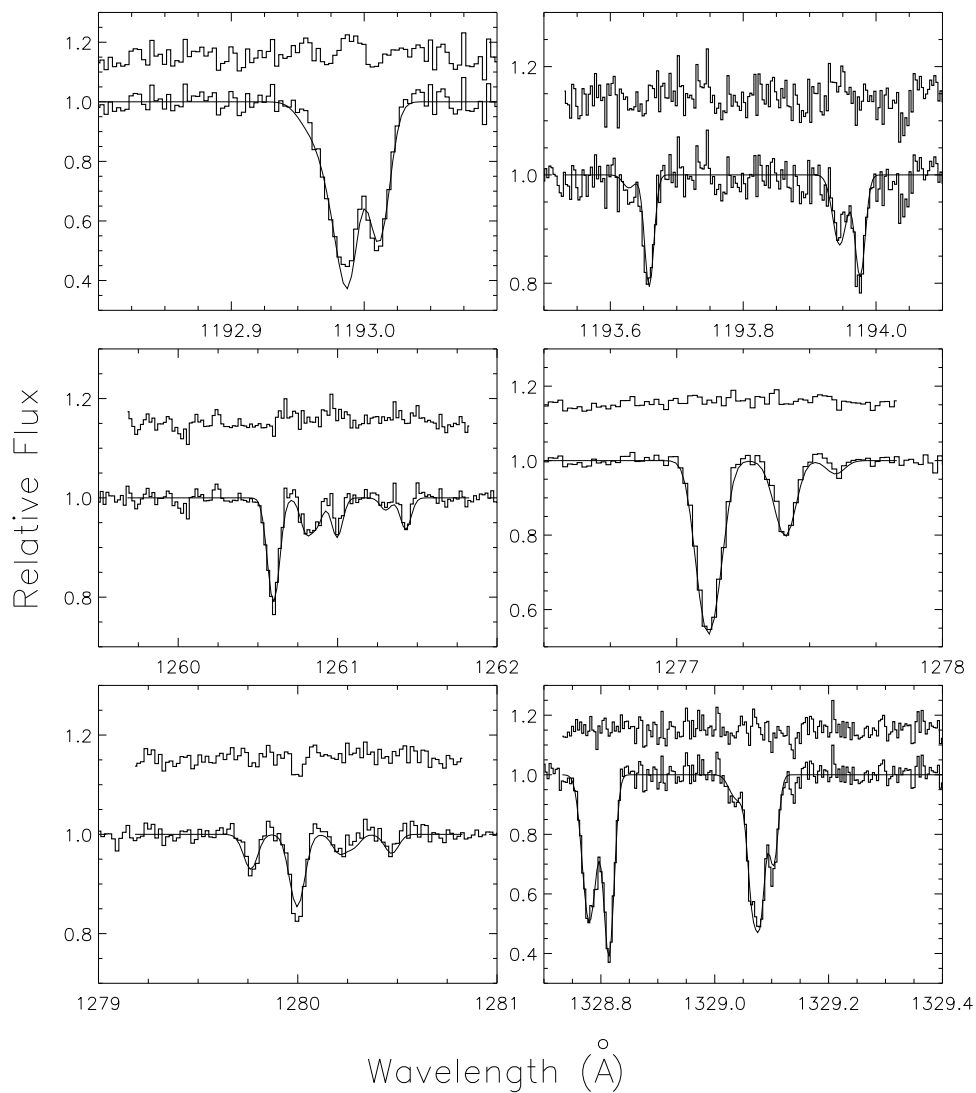


Fig. 1.— Observed (histograms) and model (lines) spectra of the C I multiplets toward 1 Sco. All spectra are medium resolution unless otherwise noted. a) The top, middle, and bottom rows from left to right show multiplets $\lambda\lambda 1193, 1194$ (high resolution), $1260, 1277, 1280$, and 1329 (high resolution, $J = 0$ and 1 levels only), respectively. The residuals are displayed above each spectra, offset by $+1.15$.

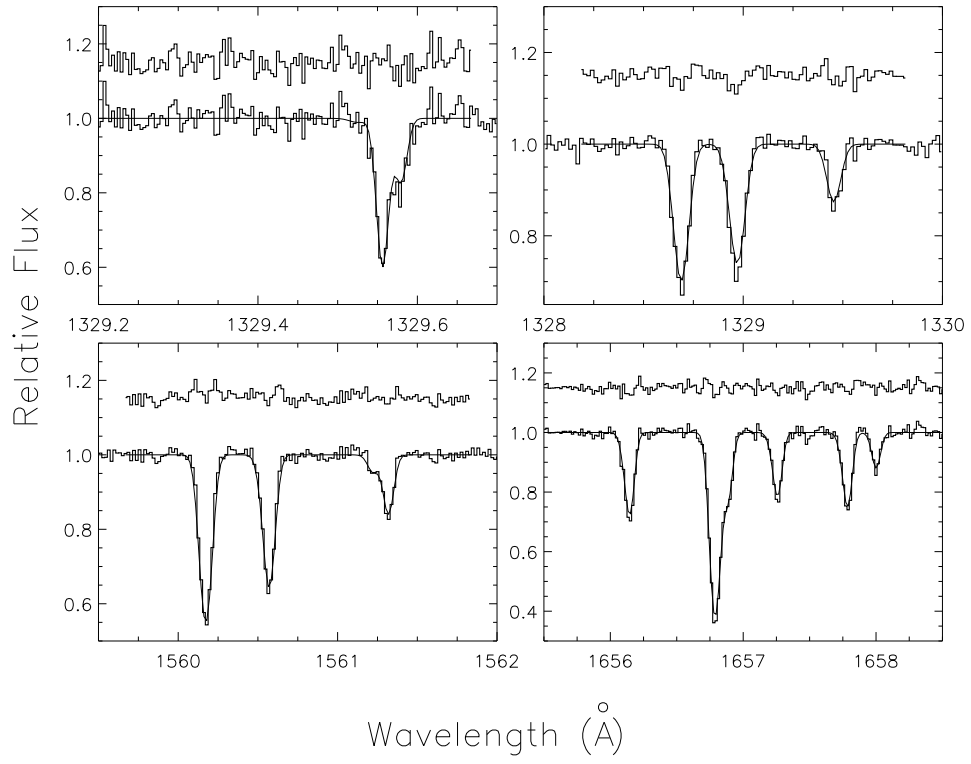


Fig. 1.— b) Spectra of multiplets $\lambda\lambda 1329$ (high resolution, $J = 2$ level only), 1329, 1561, and 1657.

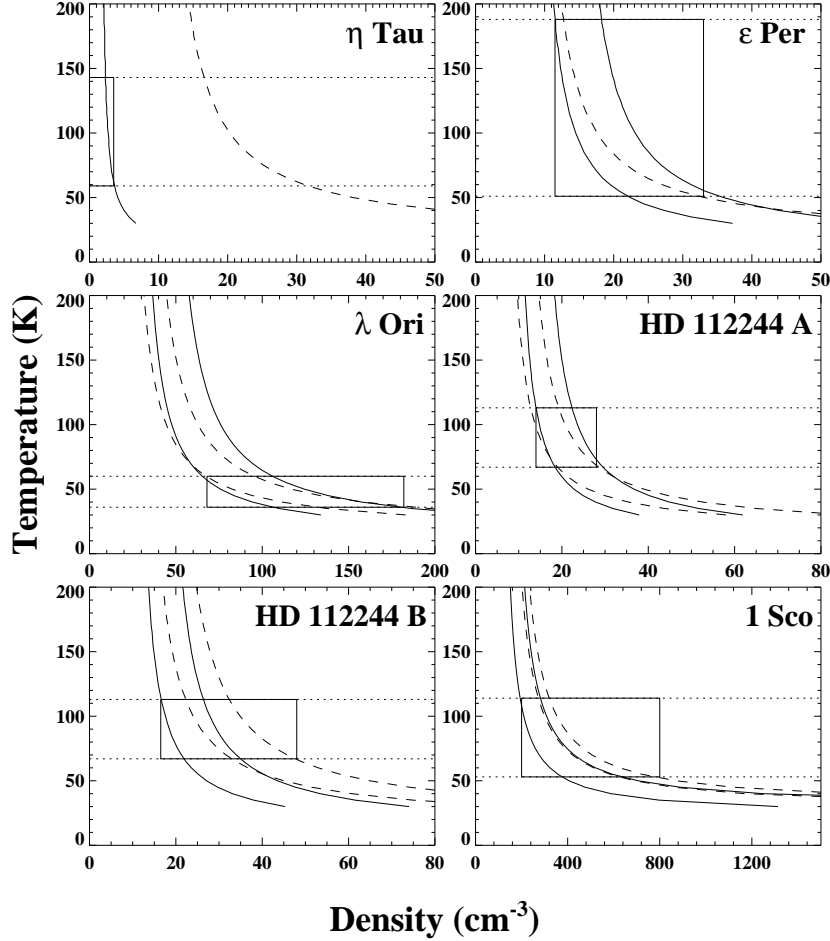


Fig. 2.— The density-temperature relationships for the main components along our sight lines. The curves for the secondary component toward HD 112244 (component B) are also displayed. The two solid lines represent the density-temperature correspondence calculated from the lowest and the highest $n_{J=1}/n_{J=0}$ ratios allowed by our C I column densities. A similar pair of lines (dashed lines) show the relationships calculated from the $n_{J=2}/n_{J=0}$ ratios. If only an upper limit was available for either the $J = 1$ or 2 column density, then a single line shows the maximum gas densities as a function of temperature for the corresponding ratio. The density-temperature values, inferred from a ratio, are between the curves belonging to the same ratio. In the cases of upper limits, all density-temperature points that are to the left of the curve are allowed. The dotted horizontal lines are the H₂ excitation temperatures from Savage et al. 1977. The thick rectangles contain all density-temperature values that are consistent with both ratios and the H₂ excitation temperatures. The overlap between the ranges was not sufficient toward HD 112244 B, 1 Sco, and β^1 Sco; in these cases, the rectangles contain the extreme density-temperature values that are consistent with all measures.

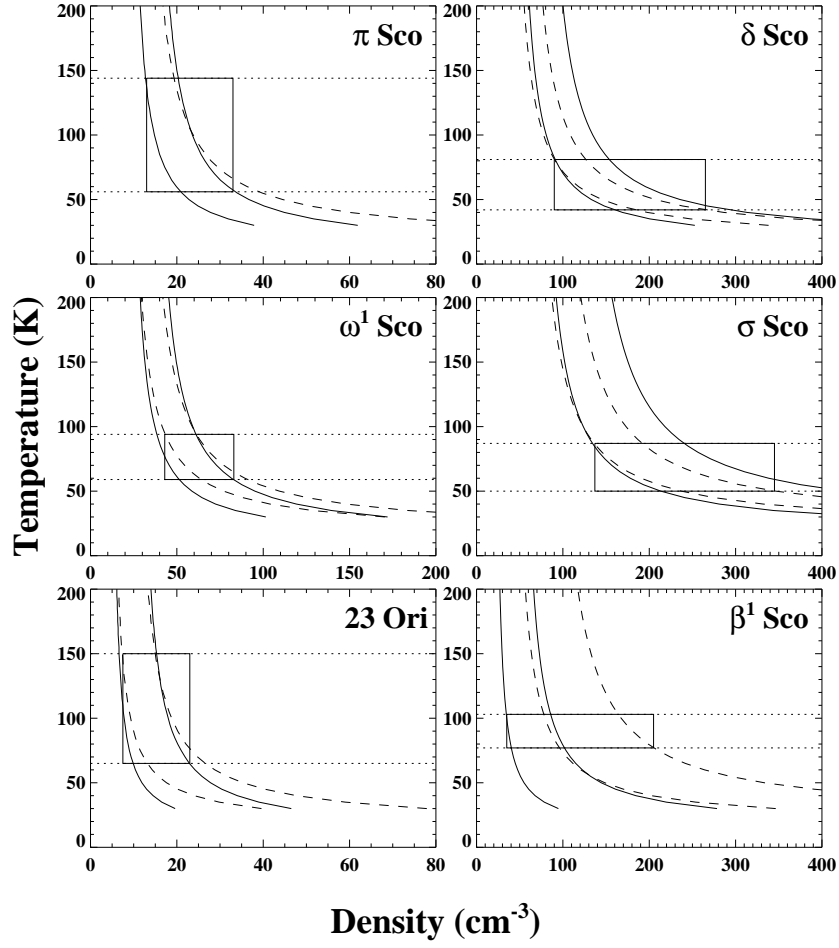


Fig. 2.— Cont.

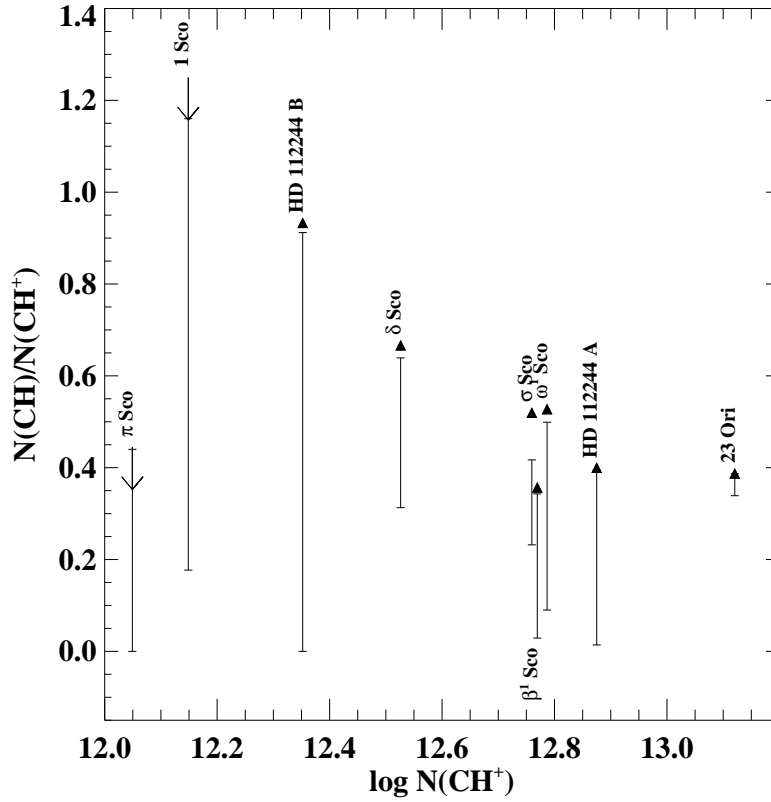


Fig. 3.— CH produced by the non-equilibrium CH^+ chemistry, normalized by the observed amount of CH^+ , as a logarithmic function of CH^+ columns. The arrows and triangles indicate the upper limits and measured amount of CH, respectively. The maximum and the minimum amount of CH associated with the CH^+ chemistry are shown by ranges. The identifier of each sight line is printed above the symbols except for β^1 Sco which is below the symbol for clarity.